ELSEVIER

Journal of Biomechanics 38 (2005) 1789–1797

JOURNAL OF BIOMECHANICS

www.elsevier.com/locate/jbiomech
www.JBiomech.com

Nanomechanics of opposing glycosaminoglycan macromolecules

Joonil Seog[a,1], Delphine Dean[b], Bernd Rolauffs[b], Tao Wu[c,2], Jan Genzer[c], Anna H.K. Plaas[d], Alan J. Grodzinsky[a,b,e], Christine Ortiz[f,*]

[a]*Department of Mechanical Engineering, Massachusetts Institute of Technology, 77 Massachusetts Avenue, MIT 13-4022, Cambridge, MA 02139, USA*
[b]*Department of Electrical Engineering and Computer Science, Massachusetts Institute of Technology, 77 Massachusetts Avenue, MIT 13-4022, Cambridge, MA 02139, USA*
[c]*Riddick Laboratories, Department of Chemical Engineering, North Carolina State University, Raleigh, NC 27695-7905, USA*
[d]*Department of Pharmacology and Therapeutics, College of Medicine, University of South Florida, Tampa, FL 33620, USA*
[e]*Biological Engineering Division, Massachusetts Institute of Technology, 77 Massachusetts Avenue, MIT 13-4022, Cambridge, MA 02139, USA*
[f]*Department of Materials Science and Engineering, Massachusetts Institute of Technology, 77 Massachusetts Avenue, MIT 13-4022, Cambridge, MA 02139, USA*

Accepted 6 September 2004

Abstract

In this study, the net intermolecular interaction force between a chondroitin sulfate glycosaminoglycan (GAG)-functionalized probe tip and an opposing GAG-functionalized planar substrate was measured as a function of probe tip–substrate separation distance in aqueous electrolyte solutions using the technique of high resolution force spectroscopy. A range of GAG grafting densities as near as possible to native cartilage was used. A long-range repulsive force between GAGs on the probe tip and substrate was observed, which increased nonlinearly with decreasing separation distance between probe tip and substrate. Data obtained in 0.1 M NaCl was well predicted by a recently developed Poisson–Boltzmann-based theoretical model that describes normal electrostatic double layer interaction forces between two opposing surfaces of end-grafted, cylindrical rods of constant volume charge density and finite length, which interdigitate upon compression. Based on these results, the nanomechanical data and interdigitated rod model were used together to estimate the electrostatic component of the equilibrium modulus of cartilage tissue, which was then compared to that of normal adult human ankle cartilage measured in uniaxial confined compression.

Keywords: Cartilage; Glycosaminoglycan; Atomic force microscopy; Electrostatic; Poisson–Boltzmann

1. Introduction

Cartilage is a highly specialized, dense connective tissue that allows the smooth movement of articulating joints (Kuettner, 1992). Approximately 50% of the tissue's equilibrium compressive modulus and swelling pressure is associated with repulsive inter- and intramolecular electrostatic interactions between the negatively charged glycosaminoglycan (GAG) constituents of the extracellular matrix (Buschmann and Grodzinsky, 1995; Eisenberg and Grodzinsky, 1985; Maroudas, 1976; Ogston, 1970), which comprise 5–10% of the tissue's wet weight (Buckwalter and Mankin, 1997a). The earliest stages of osteoarthritis involve a decrease in GAG length and loss of GAG from cartilage (Buckwalter and Mankin, 1997b). Although the tissue-level biomechanical and physicochemical properties of cartilage have been well-documented (Mow and Guo, 2002), the fine nanoscale mechanisms by which the constituent macromolecules determine tissue-level mechanical

*Corresponding author. Tel.: +1 617 452 3084; fax: +1 617 452 3085.
E-mail address: cortiz@mit.edu (C. Ortiz).
[1]Present address: The CBR Institute for Biomedical Research, Inc., Harvard Medical School, Boston, MA 02115, USA.
[2]Present address: National Institute of Standards and Technology, Polymers Division, Polymers Building (224), Room B228, 100 Bureau Drive, Stop 8546, Gaithersburg, MD 20899-8546, USA.

0021-9290/$ - see front matter © 2004 Elsevier Ltd. All rights reserved.
doi:10.1016/j.jbiomech.2004.09.010

function with age, injury and disease remain less experimentally quantified.

Both macroscopic continuum theories based on Donnan equilibrium (Lai et al., 1991; Soulhat et al., 1999) and molecular-scale Poisson–Boltzmann-based continuum theories (Buschmann and Grodzinsky, 1995; Dean et al., 2003) have been formulated to model GAG electrostatic interactions. The latter accounts for the nanometer-scale space-varying electric potential and fields between neighboring GAGs. More recently, molecular dynamics simulations have incorporated atomic-level modeling of the GAG structure to predict GAG persistence length and other biophysical parameters (Bathe et al., 2003). Additionally, investigators have developed constitutive laws to relate molecular-level models to tissue-level properties and have evaluated these models by comparison to tissue-level measurements. Experimental data on nanoscale structure and mechanical properties will aid in the development of molecular models and in the understanding of molecular mechanisms underlying tissue-level properties. Only recently have new nanoscale techniques and methodologies become available, such as tapping mode atomic force microscopy (AFM) imaging (Cowman et al., 1998; Hunziker et al., 2002; Ng et al., 2003; Raspanti et al., 2001), nanoindentation (Ferguson et al., 2003), high-resolution force spectroscopy (Seog et al., 2002), laser tweezers (Fujii et al., 2002; Liu et al., 2003), and single molecule force spectroscopy (Sasaki and Odajima, 1996; Sun et al., 2002). These methods are capable of yielding direct information on the molecular structure and nanomechanical properties of cartilage.

In this study, we have used recently reported methods to prepare end-grafted chondroitin sulfate (CS) GAG-functionalized planar substrates (Seog et al., 2002) and nanoscale probe tips (Seog et al., 2004) with a range of grafting densities close to that found in native cartilage. The interaction force (F) between a GAG-functionalized probe tip and a GAG-functionalized planar substrate was measured on approach (compression), at a constant rate, as a function of probe tip–substrate separation distance (D). In the samples studied here, the maximum surface interaction area between the probe tip and sample surface was calculated to be $\sim$1500 nm^2, corresponding to $\sim$40 GAG chains on the probe tip and $\sim$40 GAG chains on the substrate. Measurements were performed in aqueous electrolyte of varied salt concentration (0.0001–1 M NaCl) and pH (3 and 7). Data obtained in 0.1 M NaCl were compared to the predictions of a recently developed Poisson–Boltzmann-based theoretical model that describes normal electrostatic double layer interaction forces between two opposing surfaces of end-grafted, cylindrical rods of constant volume charge density and finite length, which interdigitate upon compression (Dean et al., 2003). Based on these results, this model was then used to estimate the electrostatic component of the equilibrium modulus of cartilage tissue and the predicted modulus was compared to that of normal adult human ankle cartilage measured in uniaxial confined compression.

2. Materials and methods

2.1. GAG sample preparation and characterization

Amine-terminated, metabolically radiolabeled ^{35}S-CS-GAGs were prepared from rat chondrosarcoma cell cultures, purified, and characterized as previously reported (MW$\sim$13,428 g/mol, polydispersity$\sim$1.06) (Seog et al., 2002). The GAGs were treated with 1 μM dithiobis (sulfosuccinimidyl propionate) and the internal disulfide bonds were reduced to a thiol groups using 0.1 mM dithiothreitol (Aldrich). Thiol-functionalized GAG (0.5 mg/ml) in phosphate-buffered saline (PBS) (IS = 0.15 M, pH 7.4, 0.1 wt% of sodium dodecyl sulfate) was prepared. Five microliters of this solution was placed on 1 cm × 1 cm piranha (3:1 H_2SO_4/H_2O_2 (30 wt%))-cleaned polycrystalline Au substrates (root mean square roughness, island size, and island peak-to-valley height were $\sim$1.2, $\sim$30, and $\sim$3.5 nm, respectively) for 2 and 72 h. Then, the substrates were extensively rinsed with deionized (DI) water and "backfilled" by incubation in 5 mM HS–$(CH_2)_{11}$–OH ethanol solution for 15 min to passivate that part of the Au substrate not modified with GAG. After nanomechanical experiments, the GAGs were removed from the substrate via sonication at 90 °C and their surface density was measured via scintillation counting (Seog et al., 2002). The average distance between neighboring GAGs on the substrate (s) was found to be $\sim$11 nm for the 2 h incubation time and $\sim$6.5 nm for the 72 h incubation time. Carboxyl-functionalized probe tips were prepared by immersing Au-coated Si_3N_4 cantilever probe tips (*Thermomicroscopes*, Inc. V-shaped cantilever unsharpened Microlevers, spring constant = 0.01 N/m, probe tip end-radius $R_{TIP}\sim$100 nm measured by scanning electron microscopy (SEM)) in 5 mM HS–$(CH_2)_{15}$–COOH (Aldrich) in ethanol for 24 h. GAGs were end-grafted to similar Au-coated Si_3N_4 cantilever probe tips ($R_{TIP}\sim$50 nm) by applying an electric field between the tip and a platinum electrode, spaced $\sim$100 μm from each other, while both were immersed in 1 mg/ml solution of GAG in PBS within the closed liquid cell of an AFM (Multimode IIIa, Digital Instruments, Santa Barbara, CA) for 9 h as described previously (Seog et al., 2004). The same backfilling procedure was employed for the GAG-functionalized probe tips as the GAG-functionalized planar substrates. The molecular spacing between GAGs, s, on the probe tip was found previously to be $\sim$6 nm from high-resolution force spectroscopy measurements (Seog et al.,

2004). In this procedure, the force between the GAG-functionalized probe tip and an OH-terminated alkanethiol self-assembled monolayer (SAM) planar substrate functionalized with HS–$(CH_2)_{11}$–OH (Seog et al., 2002) was compared to a Poisson–Boltzmann-based charged rod model (Dean et al., 2003) (data not shown).

2.2. Variable angle spectroscopic ellipsometry (VASE)

The height of the chemically end-grafted GAGs on the planar substrate in aqueous solution was measured using variable angle spectroscopic ellipsometry (VASE VB-250, J.A. Woollam Co., Inc., USA) with a rotating analyzer configuration. The change in polarization state of light reflected from the surface of the sample was measured via the ellipsometric angles Ψ and Δ versus wavelength (240–1000 nm) at a fixed angle of incidence (70°) between the incoming beam and the sample surface normal. Two samples with different grafting densities ($s = 6.5$ and 11 nm) were immersed in a custom-designed liquid cell, and data were collected from three different spots on each sample at each solution condition. The experiments were performed in NaCl solutions of varying pH in the following order: DI water (pH~5.6), 0.0001 M NaCl (pH~5.6), 0.001 M (pH~5.6), 0.01 M (pH~5.6), 0.015 M (pH 3), 0.015 M (pH 7), 0.1 M (pH~5.6), 1 M (pH~5.6), and 3 M (pH~5.6). The minimum time for equilibrium was 2 h. At each NaCl concentration, the GAG height at the two grafting densities was compared using a two-tailed Student's t-test.

The GAG heights were obtained by fitting the ellipsometry data to a "simple box" multilayer model to determine an average "optical" height as previously described (Wu et al., 2003). The GAG end-grafted surface was modeled as three homogeneous layers: gold, hydrated GAG layer, and a fluid environment. The assumption of uniformity of the GAG layer was supported by the low standard deviations in the nanomechanical measurements (<20 pN) at a variety of different locations on the sample surface. The ellipsometry data were fit by varying the GAG layer thickness with fixed refractive indices for two of the layers: GAG layer = 1.346 and salt water (0.1 M NaCl) = 0.395 (both of which are the real components and the imaginary components are equal to zero). For the gold layer, known values for the real and imaginary parts of the refractive index as a function of wavelength were included in the analysis. The refractive index of the GAG (1.346) was independently obtained from GAG solution measurement using a refractometer (ABBE-3L, Spectroscopic Instruments, Woburn, MA). Regression algorithms were used to vary GAG layer thickness as an unknown parameter and minimize the difference of square root of $(\psi^2 + \Delta^2)$ between experimental data and theoretical data generated from the simple box model, using the WVASE32 instrument software. While the actual values of the GAG height have been shown to deviate slightly (up to ~5%) with the particular model employed, the trends observed with varying solution conditions appear the same regardless of the model used (Wu et al., 2003).

2.3. Nanomechanical experiments

High-resolution force spectroscopy between GAG-functionalized substrates and carboxyl or GAG-functionalized probe tips was conducted using a cantilever-based instrument called the Molecular Force Probe (MFP, Asylum Research, Inc.) to measure force (F, nN) versus tip–sample separation distance (D, nm) in aqueous solutions at room temperature (Fig. 1a) (Seog et al., 2002). The spring constant for each experiment was determined according to the nondestructive thermal oscillation method described in the literature (Hutter and Bechhoefer, 1993). The z-piezo rate of displacement was $z = 1$ μm/s; the measured force did not vary with approach tip velocity in the range 0.2–2 μm/s, suggesting

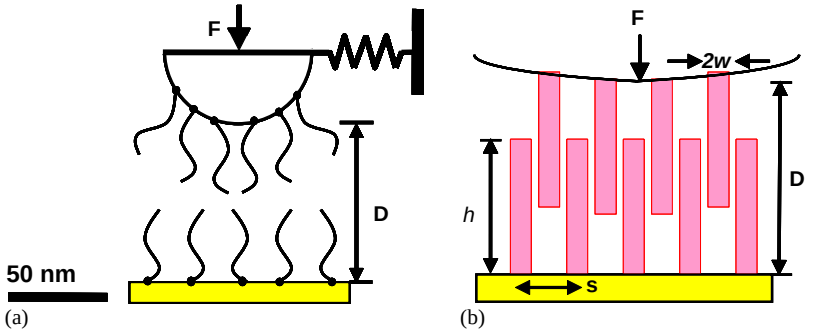

Fig. 1. (a) Schematic of the nanomechanical experiment to measure the interaction force between a GAG-functionalized probe tip and GAG end-grafted Au-coated substrate. GAG conformation and height h vary with bath solution salt concentration and pH. GAG contour length $L_{contour}$~45 nm, inter-GAG spacing s~6.5 nm for a 72 h chemisorption reaction time, and the probe tip end-radius, R_{TIP}~50 nm. The HS–$(CH_2)_{11}$–OH SAM molecules used for backfilling are not shown and are ~1 nm in height. (b) Schematic of interdigitated charged rod model used to describe the nanomechanical experiment.

that measured forces correspond to the quasi-static regime in this configuration (data not shown). Further evidence was provided by an estimation of the hydrodynamic drag force which is defined as $F_{drag} = \xi z$ where ξ (pN s/nm) is a drag coefficient. ξ has been approximated for typical experiments employing AFM cantilever probe tips in aqueous solution to be of the order $\xi \sim 10$–3 pN s/nm (Evans, 2001). For the $z = 1$ μm/s used in the force spectroscopy experiments reported here, F_{drag} is calculated to be 1 pN which is below the thermal limit of force detection of the nanomechanical device (~5 pN for the specific cantilevers used). In addition, F_{drag} is also equivalent to the offset between the approach and retract curves at distances greater than the surface forces interaction regime (Hoh and Engel, 1993). Using this definition, F_{drag} was observed to be experimentally negligible in all force spectroscopy experiments performed and reported here. Nanomechanical data presented are averaged curves of 10–15 individual experiments on approach of the probe tip normal to the sample surface at different sample locations, and have a standard deviation < 20 pN. The linear constant compliance region corresponding to contact with the underlying Au substrate was clearly observed and set to $D = 0$. Force/radius = R_{TIP} was reported in order to present a normalized effective energy of interaction and allow for approximate comparison of datasets taken with different probe tips.

Stress was calculated as the force normalized by the projected tip area on the flat substrate, $\sigma = F/[\pi R_{TIP}^2]$. Strain, ε, was estimated as the second-order function, $\varepsilon = [1 - (D/h)^2]$, thus representing the experiment as a two-dimensional compression of opposing GAGs, with $D = h$ taken to be the undeformed, zero-strain length scale. Modulus was calculated as the derivative of the stress with respect to strain.

2.4. Macroscopic tissue biomechanical experiments

The equilibrium modulus of full thickness human ankle (talar dome) cartilage specimens was measured in uniaxial confined compression in PBS (IS~0.15 M, pH 7.4) using previously established methods (Treppo et al., 2000) with tissue from two different donors (56 and 62 years of age, both normal Collin's grade 0). Using an incubator-housed loading apparatus, sequential ramp-and-hold compressions were applied individually to three cylindrical disk specimens from each donor. Following each ramp compression, stress relaxation ensued and the final equilibrium stress was measured at each equilibrium strain in the 0–0.6 range. Human tissue was obtained from the Gift of Hope Organ Donor Network (Elmhurst, IL) and research was approved by the Committee on Use of Humans as Experimental Subjects at MIT.

2.5. Theoretical modeling

Nanomechanical data were compared to the predictions of a charged-rod Poisson–Boltzmann (PB) model for electrostatic double layer forces as described previously (Dean et al., 2003). The time-averaged space occupied by an individual CS-GAG chain and its fixed charge groups was represented by a circular cylinder having height, h, (which was set equal to the experimentally measured GAG height) effective rod radius, w, and a fixed uniform volume charge density (Fig. 1b). Opposing cylinders interdigitate as they are brought together on approach and, for $D < h$, each rod deforms while maintaining a constant volume. The PB equation was solved numerically in a plane parallel geometry to find the electrical potential, Φ, in all space using a Newton method on finite difference grid (Dean et al., 2003). Φ was then used to calculate the electrostatic free energy, and the force was calculated as the derivative of the free energy with respect to distance perpendicular to the sample plane. The probe tip geometry was approximated as a hemisphere by using the calculated force between the planar surfaces and summing up the force on appropriately sized concentric cylinders. Based on biochemical and biophysical measurements on rat chondrosarcoma GAGs, the average GAG chain was assumed to be 25 disaccharides long (Dean et al., 2003). Therefore, the following fixed parameters values were used in the model: total GAG (cylinder) charge, $Q_{rod} = 8 \times 10^{-18}$ C (assuming one ionized COO^- and SO_3^- group per disaccharide); probe tip end-radius $R_{TIP} = 50$ nm (Seog et al., 2004); $h = 45$ nm (measured by VASE at 0.1 M NaCl), effective rod radius, $w = 2$ nm, and inter-GAG spacing, $s = 6$–7 nm (measured by scintillation counting).

3. Results

3.1. Characterization of GAG-functionalized substrates of differing grafting densities

3.1.1. Spectroscopic ellipsometry

The GAG height, h, was measured by VASE for two different grafting densities (2 and 72 h chemisorption reaction times corresponding to $s \sim 11$ nm and $s \sim 6.5$ nm, respectively) as a function of NaCl concentration at pH~5.6 (Fig. 2a). For the 72 h sample, h increased from ~20 (pure DI water) to ~28 nm (0.0001 M NaCl), and then remained relatively unchanged up to 0.01 M NaCl. The 2 h sample showed the same trend with NaCl concentration, but h was ~10 nm less than that of the 72 h sample at each NaCl concentration. The maximum h occurred at 0.1 M NaCl (43 and 37 nm for the 72and 2 h chemisorption reaction time, respectively), and in both samples h decreased with further increases in NaCl

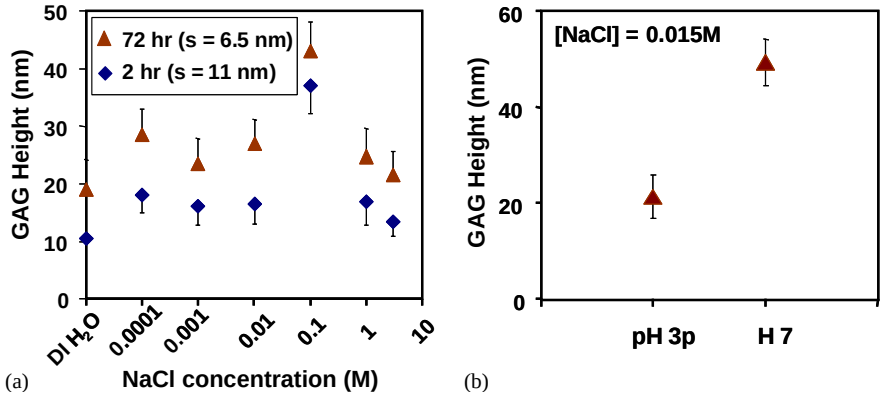

Fig. 2. (a) Ellipsometric measurement of end-grafted GAG height versus bath NaCl concentration at pH~5.6 for two different chemisorption reaction times (2 h (–◆–) and 72 h (–▲–) corresponding to s~11 nm and s~6.5 nm, respectively); (b) end-grafted GAG height at pH 3 versus pH 7, bath [NaCl] = 0.015 M, using a 72 h chemisorption reaction time (–▲–). Data are mean ± SD.

up to 3 M. The difference in h between the two grafting density samples was statistically significant ($p<0.05$) except at 0.1 M NaCl. At pH 7, h (48 nm) was significantly different than that at pH 3 (23 nm, $p<0.05$), suggesting that a conformational change occurred in the GAGs due to the increased ionization state of the GAG carboxyl groups at pH 7 (Fig. 2b). The pKa of the carboxylic acid group is ~3.5 (Freeman and Maroudas, 1975), while that of the sulfate group is ~2 (Kuettner and Lindenbaum, 1965); thus, the fixed charge density of CS-GAG is higher at pH 7 than at pH 3 due to deprotonation of GAG carboxylic groups. At pH~5.6, the carboxyl groups are fully ionized except at the lowest ionic strengths ($\leqslant$0.001 M) at which partial protonation may occur (Frank et al., 1990).

3.1.2. Nanomechanical characterization

The force on approach between a carboxyl-terminated SAM probe tip and the two GAG-functionalized substrates of differing grafting densities (s~11 and 6.5 nm) in 0.001 M NaCl, pH~5.6, was nonlinear and purely repulsive (Fig. 3). For the sample having s~6.5 nm, the distance at which the repulsive force began to increase was twice as long as the GAG contour length, indicating that long-range electrostatic double layer interactions play a role. At both grafting densities, the force profiles were nonhysteretic, suggesting that chemically end-grafted GAG layers remain stable and have minimal interaction with the substrate during repeated force measurements. No van der Waals jump-to-contact at the top of the GAG layer or the underlying Au substrate was observed, indicating that the GAG grafting densities obtained were enough to shield attractive surface interaction between the probe tip and substrate. At 10 nm from the surface, the magnitude of the force with the higher GAG grafting density was 6 × higher than that with the lower density; thus, grafting density directly affected the magnitude of the

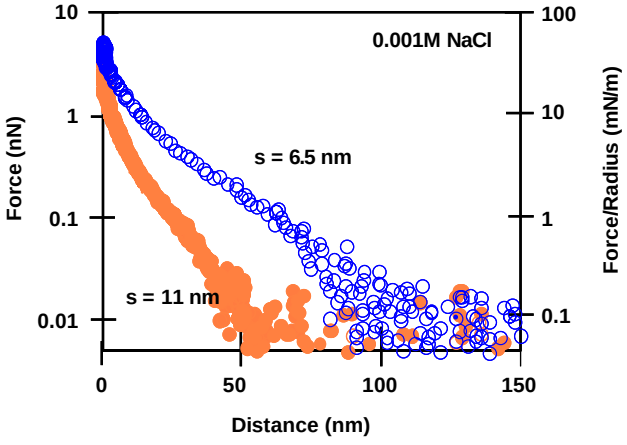

Fig. 3. Force versus separation distance at 0.001 M NaCl concentration, pH~5.6, for a COO^--terminated SAM functionalized probe tip (R_{TIP}~100 nm) versus GAG end-grafted substrates made with 2 h (s~11 nm, ●) and 72 h (s~6.5 nm, –○–) chemisorption times.

electrostatic repulsive force, likely due to intra- and intermolecular GAG–GAG interactions at the higher grafting density.

3.2. Nanomechanical experiments between opposing GAG layers

The force between two opposing GAG layers (s~6.5 nm) was measured at NaCl concentrations from 0.0001 to 1.0 M at pH~5.6 (Fig. 4a). In 0.0001 M NaCl, long range, nonlinear repulsive forces were observed to start at D~150 nm, which is longer than twice the fully extended contour length of the GAGs calculated from their known MW~13,428 ($L_{contour}$~45 nm). At 1 M NaCl, the force started at D~40 nm; at all NaCl concentrations, the force increased monotonically to a maximum of ~1 nN at $D = 0$ (Force/radius ~10 mN/m) just prior to reaching the constant compliance region.

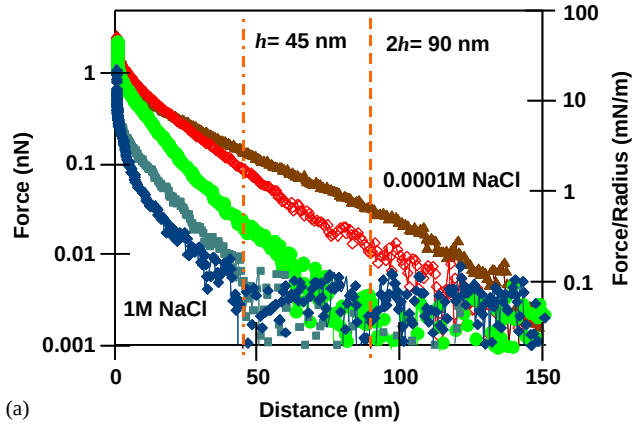

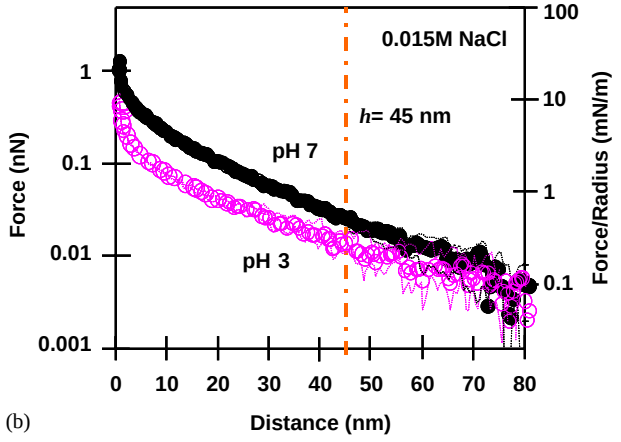

Fig. 4. Force versus separation distance for a GAG-functionalized probe tip versus GAG-functionalized planar substrate with $s\sim6.5$ nm (a) at pH$\sim$5.6 and varying NaCl concentrations: (–▲–) 0.0001 M, (–◇–) 0.001 M, (–●–) 0.01 M, (–□–) 0.1 M, and (–♦–)1 M; (b) 0.015 M NaCl at pH 3 (data: ○, standard deviation: ⋯⋯) and pH 7 (data: ●, standard deviation: ⋯⋯).

These profiles again showed no van der Waals jump-to-contact at the top of the GAG layers or the underlying Au substrate, and no hysteresis or adhesion on retraction of the probe tip away from the surface. The range and magnitude of the repulsion decreased with increasing ionic strength, consistent with salt screening of electrostatic repulsion forces. Additional experiments (Fig. 4b) at two different pH values (3 and 7) but at constant ionic strength (0.015 M NaCl) showed a substantial decrease in force at pH 3 compared to pH 7, consistent with the lower GAG charge density at pH 3. The ionic strength and pH dependence (Fig. 4a,b) suggest that electrical double layer repulsion is the major component of the net interaction between opposing GAGs for the experimental conditions used.

The data at 0.1 M NaCl (Fig. 4a) were compared to the predictions of a Poisson–Boltzmann-based theoretical model that describes normal interaction forces between two opposing surfaces of end-grafted rods of constant volume charge density and finite length, which

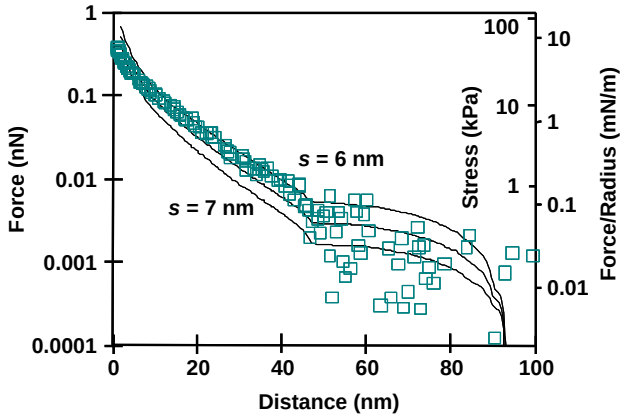

Fig. 5. Force versus separation distance for a GAG-functionalized probe tip versus GAG-functionalized planar substrate with $s\sim6.5$ nm at pH ~5.6, 0.1 M NaCl (□) compared to the predictions of the interdigitated charged rod model (—) with parameter values fixed at: [NaCl]= 0.1 M, $R_{TIP} = 50$ nm, $h = 45$ nm, $w = 2$ nm, $s = 6-7$ nm, $Q_{rod} = -8 \times 10^{-18}$ C.

deform by interdigitating (Fig. 1b) (Dean et al., 2003). Model parameter values were fixed at their known values obtained from independent characterization techniques (see Materials and Methods Section) and the inter-rod separation distance was set to $s = 6-7$ nm. At $D = 85$ nm, the model predicted a slight inflection point corresponding to the edges of the two GAG layers making contact with each other (Fig. 5). In the interdigitation regime ($45 < D < 85$ nm), the measured force is very low and approaching the resolution limit of instrumentation; thus, a quantitative comparison between model and experiment was difficult. At $D = 45$ nm (i.e., $D = h$) another inflection point was predicted by the model corresponding to the point where the top of the rods begin to hit the hard-walled substrate. At this position, the effective rod radius, w, begins to increase as D decreases such that the rod maintains a constant volume. For $D < 45$ nm, the most physiologically relevant strain regime, the theoretically predicted force matched the data well for reasonable model parameter values, especially for $s = 6$ nm.

4. Discussion

GAG-functionalized substrates of different grafting densities were prepared by varying the chemisorption incubation time of GAG on Au-coated substrates. The end-grafted GAG substrates were characterized by scintillation counting to estimate the average molecular separation distance between GAGs (Seog et al., 2002), VASE to estimate h as a function of ionic strength and pH (Wu et al., 2003), and nanomechanical measurements (Fig. 3) to verify consistent changes in force with variations in grafting density (Seog et al., 2002). The molecular separation distance between GAGs on the

electrically functionalized probe tip was estimated to be ~6 nm using a protocol described previously (Seog et al., 2004). Taken together, these methods enabled direct experimental measurement and interpretation of forces between an array of ~40 GAGs on the substrate and ~40 GAGs on the probe tip, thereby simulating the interaction between GAGs of adjacent aggrecan molecules in cartilage extracellular matrix (ECM), consistent with the objective of probing molecular level biomechanical interactions relevant to tissue ECM function. Strong, opposing GAG–GAG repulsion forces were found to be long range (Fig. 4) and well represented by a GAG–GAG interdigitation model as opposing GAGs came into close proximity (Fig. 5).

4.1. Conformation of end-grafted GAGs on gold substrates

The observed variation of GAG extension (height) with NaCl concentration and pH (Fig. 2) is consistent with the expected titration behavior of CS-GAGs and the effects of salt screening on molecular conformation. In DI water, the acidic groups of GAGs tend to remain protonated (uncharged) since the concentration of mobile dissociated H^+ ions would not be sufficient to simultaneously satisfy electroneutrality and equilibrium Boltzmann partitioning in the absence of other neutral salt ions such as Na^+. Thus, the non-ionized GAGs do not attain an extended conformation at very low salt concentration, and their height remains low (Fig. 2a). As NaCl concentration increases, Na^+ ions can exchange with dissociated H^+ ions and ionization of GAG charge groups occurs freely; intra- and intermolecular electrostatic repulsion leads to an extended GAG conformation and a concomitant increase in h. At very high NaCl concentration, electrostatic repulsion interactions are screened causing a decrease in h. The effect of charge density on GAG height was also clearly demonstrated via bath pH experiment (Fig. 2b). Changing pH from 3 to 7 essentially doubled h, reaching a value close to the GAG contour length (~45 nm), indicating that the GAGs were fully extended due to increased repulsive interactions between charge groups at pH 7. The measured force between the GAG substrate and negatively charged carboxyl-functionalized probe tip (Fig. 3) gave further confirmation of the presence of GAG on the substrate and the direct effect of GAG density on the repulsive force.

4.2. Nanomechanical experiments between opposing GAGs

As expected, the strong dependence of the measured GAG–GAG interaction force on ionic strength and pH (Fig. 4) suggested that electrostatic repulsion dominates these interactions. A comparison of the nanomechanical results (Figs. 3 and 4) and previous data (Seog et al., 2002, 2004) shows that repulsion between opposing GAG chains occurs over a longer range than that between a GAG-functionalized substrate and charged tip or a GAG-functionalized tip and charged substrate under physiological condition (0.1 M NaCl). Qualitatively, the deformation of opposing GAGs (Fig. 1b) may mimic certain aspects of intratissue loading in which the substrate and tip act as boundary conditions in two dimensions similar to that provided by aggrecan core protein and other ECM molecules in three dimensions.

We further explored the implications of these measurements to tissue-level mechanical properties. Using the nanomechanical data and theoretical predictions (Fig. 5) at 0.1 M NaCl, pH~5.6, the component of an effective compressive modulus associated with GAG–GAG electrostatic interactions as a function of normal (compressive) strain for the GAG density corresponding to s~6 nm was calculated (Fig. 6a). The

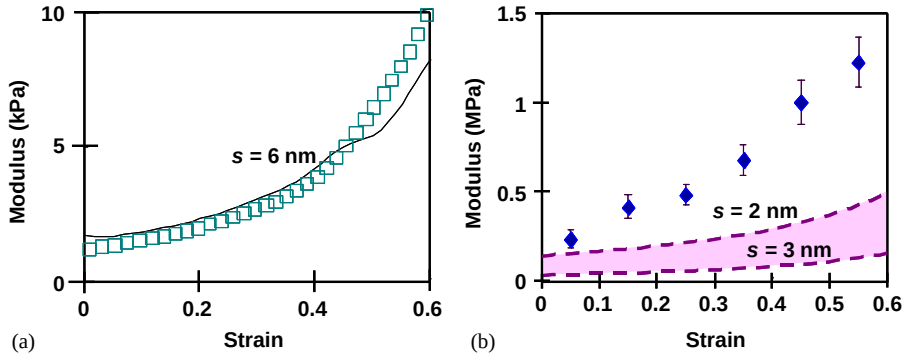

Fig. 6. (a) Effective compressive modulus associated with GAG–GAG interactions calculated from nanomechanical data (□) of Fig. 5 (pH~5.6, 0.1 M NaCl) versus compressive strain, ε, estimated from $\varepsilon = 1-(D/h)^2$; the GAG–GAG modulus is compared to the prediction of the interdigitated charged rod model ($s = 6$ nm) (—). (b) Equilibrium compressive modulus of human ankle cartilage measured in confined compression (♦) in PBS (ionic strength ~0.15 M, pH 7.4) compared to the component of the modulus predicted by interdigitated charged rod model of GAG–GAG electrostatic repulsive interactions with parameters values $s = 2-3$ nm, $h = 30$ nm, $w > 0.5$ nm (shaded region inside – –). Data are mean ± SD.

resulting electrostatic component of the modulus increased nonlinearly with compressive strain, ε reaching a maximum value of $\sim$10 kPa at $\varepsilon = 0.6$. The interdigitating charged rod model predicted the trends of the strain-dependent GAG-interaction modulus very closely for reasonable values of model parameters (Fig. 6a). The small inflection observed in the model prediction at $\varepsilon \sim 0.45$ is due to the change in slope of the force profile that occurs as the rods transition from approaching and interdigitating at constant volume (and constant charge density) to the position at which the rods have expanded to fill their individual unit cells and further compression causes the volume charge density to increase with decreasing separation distance. This inflection was not observed in the nanomechanical data, suggesting that there is no such sharp transition between regimes in the experiment.

4.3. Comparison of GAG–GAG experiment and model to cartilage tissue biomechanical data

The equilibrium modulus of cylindrical disks of normal adult human ankle cartilage measured in confined compression was $\sim$0.25–0.5 MPa in the 0.05–0.25 strain range (Fig. 6b) and increased to $\sim$1.2 MPa by 0.60 strain. In cartilage tissue, GAG electrostatic forces have been shown to account for 50% of the total modulus (Eisenberg and Grodzinsky, 1985). However, the experimentally measured modulus values of ankle cartilage were $\sim$2 orders of magnitude greater than the estimated modulus calculated from the GAG versus GAG nanomechanical experiments. This disparity is most likely due to the fact that the GAG density in the nanomechanical experiments (Fig. 4) was $\sim$4 times smaller than the known GAG density in human ankle tissue (Treppo et al., 2000). (All GAG fixed charge groups are ionized under the pH and IS conditions of both the macroscopic tissue measurements (Frank et al., 1990) and molecular mechanics measurements.). The component of the modulus attributed to GAG–GAG electrostatic repulsive interactions was recomputed using the charged rod model with a range of model parameters known to include values reported for adult GAG and aggrecan cartilage (i.e., $s = 2-3$ nm, $h = 30$ nm) (Ng et al., 2003). The results (Fig. 6b) show that the GAG–GAG component is predicted to be $\frac{1}{3}-\frac{1}{2}$ that of the measured tissue modulus. This finding is consistent with previous experiments showing that electrostatic interactions account for $\sim$50% of the total compressive modulus of cartilage (Eisenberg and Grodzinsky, 1985), and that the compressive modulus of cartilage is generally proportional to its GAG content (Williamson et al., 2001). Finally, the contribution of GAG–GAG steric interactions to the modulus of cartilage has been previously estimated to be less than 10–15% for tissue-level GAG densities (Kovach, 1995), This is consistent with our own previous measurement and modeling of GAG–GAG interactions suggesting dominance of electrostatic repulsive interactions (Dean et al., 2003). While steric interactions may become more important at very high compressive strains, we tested that hypothesis here that electrostatic interactions alone may be sufficient to explain the contribution of GAG–GAG interactions to the tissue modulus. In addition, that it may be possible to explore the consequences of specific nanomolecular structural parameters on tissue level properties using such an approach.

Thus, the comparison between theory and experiment (Fig. 6b) exemplifies a bridge between molecular level structure and tissue level biomechanical properties. Of course, values for GAG structural parameters (e.g., s and h) will clearly vary with cartilage species, age, and location. A limitation of our comparison is that the GAGs were from rat chondrosarcoma cells while the tissue was from adult human ankle. The rationale was the need to use well-characterized metabolically labelled ^{35}S-GAGs derived from a high-density cell culture, since this was the only way to achieve radiolabel specific activity that was high enough to enable assessment of GAG grafting density. In addition, human aggrecan has an abundance of keratan sulfate (KS) in the CS-GAG domain, which may contribute to electrostatic interactions, as well as to the spacing between CS-GAG chains along the core protein (Calabro et al., 2001). Ongoing studies are aimed at the combined use of experiment and theoretical modeling to address such issues. Additional studies focus on measurement of nanomolecular interactions between whole aggrecan molecules. The dependence of the measured nanomechanical force on aggrecan structure and the location of the charge along the GAG molecules will again depend on tissue age and disease state, and can be directly compared to the properties of the parent normal or osteoarthritic tissue using the methods similar to those described here. In summary, unique nonlinear, long-range repulsive behavior was observed in the direct measurement of GAG–GAG interactions, and comparison with a Poisson–Boltzmann-based polyelectrolyte "charged rod" model for electrostatic double layer interactions provided strong evidence that nonplanar charge distributions and lateral electrostatic interactions of GAG macromolecules play a major role in the observed molecular interactions.

Acknowledgements

Supported by NIH Grant AR33236, the Dupont-MIT Alliance, and a Whitaker Foundation graduate fellowship (DD).

References

Bathe, M., Rutledge, G.C., Grodzinsky, A.J., Tidor, B., 2003. Towards a multi-scale model of cartilage: coarse-graining glycosaminoglycans. In: Bathe, K.J. (Ed.), Second MIT Conference on Computational Fluid and Solid Mechanics. Elsevier, Cambridge, MA, pp. 1626–1630.

Buckwalter, J.A., Mankin, H.J., 1997a. Instructional course lectures, the American Academy of Orthopaedic Surgeons—articular cartilage. Part I: Tissue design and chondrocyte–matrix interactions. Journal of Bone and Joint Surgery, American Volume 79, 600–611.

Buckwalter, J.A., Mankin, H.J., 1997b. Instructional course lectures, the American Academy of Orthopaedic Surgeons—articular cartilage. Part II: Degeneration and osteoarthrosis, repair, regeneration, and transplantation. Journal of Bone and Joint Surgery, American Volume 79, 612–632.

Buschmann, M.D., Grodzinsky, A.J., 1995. A molecular model of proteoglycan-associated electrostatic forces in cartilage mechanics. Journal of Biomechanical Engineering 117 (2), 179–191.

Calabro, A., Midura, R.J., Wang, A., West, L.A., Plaas, A.H.K., Hascall, V.C., 2001. Fluorophore-assisted carbohydrate electrophoresis (FACE) of glycosaminoglycans. Osteoarthritis and Cartilage 9 (SA), S16–S22.

Cowman, M.K., Lin, M., Balazs, E.A., 1998. Tapping mode atomic force microscopy of hyaluronan: Extended and intramolecularly interacting chains. Biophysical Journal 75, 2030–2037.

Dean, D., Seog, J., Ortiz, C., Grodzinsky, A.J., 2003. A new molecular-level theoretical model for the electrostatic interactions between polyelectrolyte macromolecules using glycosaminoglycans as a model system. Langmuir 19 (13), 5526–5539.

Eisenberg, S.R., Grodzinsky, A.J., 1985. Swelling of articular cartilage and other connective tissues: Electromechanochemical forces. Journal of Orthopaedic Research 3 (2), 148–159.

Evans, E., 2001. Probing the relation between force-lifetime and chemistry in single molecular bonds. Annual Review of Biophysical and Biomolecular Structure 30, 105–128.

Ferguson, V.L., Bushby, A.J., Boyde, A., 2003. Nanomechanical properties and mineral concentration in articular calcified cartilage and subchondral bone. Journal of Anatomy 203 (2), 191–202.

Frank, E.H., Grodzinsky, A.J., Phillips, S.L., Grimshaw, P.E., 1990. Physicochemical and bioelectrical determinants of cartilage material properties. In: Mow, V.C., Ratcliffe, A., Woo, S.L.-Y. (Eds.), Biomechanics of Diarthrodial Joints. Springer, New York, pp. 261–282.

Freeman, W.D.S.C., Maroudas, A., 1975. Charged group behaviour in cartilage proteoglycans in relation to pH. Annals of the Rheumatic Diseases 34, 44–45.

Fujii, T., Sun, Y.L., An, K.N., Luo, Z.P., 2002. Mechanical properties of single hyaluronan molecules. Journal of Biomechanics 35 (4), 527–531.

Hoh, J.H., Engel, A., 1993. Friction effects on force measurements with an atomic force microscope. Langmuir 9, 3310–3312.

Hunziker, P.R., Stolz, M., Aebi, U., 2002. Nanotechnology in medicine: moving from the bench to the bedside. Chimia 56 (10), 520–526.

Hutter, J.L., Bechhoefer, J., 1993. Calibration of atomic-force microscope tips. Journal of Review of Scientific Instruments 64, 1868–1873.

Kovach, I.S., 1995. The importance of polysaccharide configurational entropy in determining the osmotic swelling pressure of concentrated proteoglycan solution and the bulk compressive modulus of articular cartilage. Biophysical Chemistry 53, 181–187.

Kuettner, K.K., 1992. Articular Cartilage and Osteoarthritis. Lippincott Williams & Wilkins, Philadelphia, PA.

Kuettner, K., Lindenbaum, A., 1965. Analysis of mucopolysaccharides in partially aqueous media. Biochimica et Biophysica Acta 101, 223–225.

Lai, W.M., Hou, J.S., Mow, V.C., 1991. A triphasic theory for the swelling and deformation behaviors of articular cartilage. Journal of Biomechanical Engineering 113, 245–258.

Liu, X., Noble, P.C., Luo, Z.P., 2003. A method for testing compressive properties of single proteoglycan aggregates. Biochemical and Biophysical Research Communications 307 (2), 338–341.

Maroudas, A., 1976. Balance between swelling pressure and collagen tension in normal and degenerate cartilage. Nature 260, 808–809.

Mow, V., Guo, X.E., 2002. Mechano-electrochemical properties of articular cartilage: Their inhomogeneities and anisotropies. Annual Review of Biomedical Engineering 4, 175–209.

Ng, L.J., Plaas, A.H.K., Sandy, J.D., Grodzinsky, A.J., Ortiz, C., 2003. Individual cartilage aggrecan macromolecules and their constituent glycosaminoglycans visualized via atomic force microscopy. Journal of Structural Biology 143 (3), 242–257.

Ogston, A.G., 1970. In: Balazs, E.A. (Ed.), Chemistry and Molecular Biology of the Intercellular Matrix. Academic Press, New York, pp. 1231–1240.

Raspanti, M., Congiu, T., Guizzardi, S., 2001. Tapping-mode atomic force microscopy in fluid of hydrated extracellular matrix. Matrix Biology 20, 601–604.

Sasaki, N., Odajima, S., 1996. Elongation mechanism of collagen fibrils and force–strain relations of tendon at each level of structural hierarchy. Journal of Biomechanical Engineering 29, 1131–1136.

Seog, J., Dean, D., Plaas, A.H.K., Wong-Palms, S., Grodzinsky, A.J., Ortiz, C., 2002. Direct measurement of glycosaminoglycan intermolecular interactions via high-resolution force spectroscopy. Macromolecules 35 (14), 5601–5615.

Seog, J., Dean, D., Frank, E., Ortiz, C., Grodzinsky, A.J., 2004. Preparation of end-grafted polyelectrolytes on nanoscale probe tips using an electric field. Macromolecules 37 (3), 1156–1158.

Soulhat, J., Buschmann, M.D., Shirazi-Adl, A., 1999. A fibril network reinforced biphasic model of cartilage in uniaxial compression. Journal of Biomechanical Engineering 121, 340–347.

Sun, Y.L., Luo, Z.P., Fertala, A., An, K.N., 2002. Direct quantification of the flexibility of type I collagen monomer. Biochemical and Biophysical Research Communication 295 (2), 382–386.

Treppo, S., Koepp, H., Quan, E.C., Cole, A.A., Kuettner, K.E., Grodzinsky, A.J., 2000. Comparison of biomechanical and biochemical properties of cartilage from human knee and ankle. Journal of Orthopaedic Research 18, 739–748.

Williamson, A., Chen, A., Sah, R., 2001. Compressive properties and function-composition relationships of developing bovine articular cartilage. Journal of Orthopaedic Research 19, 1113–1121.

Wu, T., Efimenko, K., Vlcek, P., Subr, V., Genzer, J., 2003. Formation and properties of anchored polymers with a gradual variation of grafting densities on flat substrates. Macromolecules 36, 2448–2453.